

Lab on a Chip

Accepted Manuscript



This is an *Accepted Manuscript*, which has been through the Royal Society of Chemistry peer review process and has been accepted for publication.

Accepted Manuscripts are published online shortly after acceptance, before technical editing, formatting and proof reading. Using this free service, authors can make their results available to the community, in citable form, before we publish the edited article. We will replace this *Accepted Manuscript* with the edited and formatted *Advance Article* as soon as it is available.

You can find more information about *Accepted Manuscripts* in the [Information for Authors](#).

Please note that technical editing may introduce minor changes to the text and/or graphics, which may alter content. The journal's standard [Terms & Conditions](#) and the [Ethical guidelines](#) still apply. In no event shall the Royal Society of Chemistry be held responsible for any errors or omissions in this *Accepted Manuscript* or any consequences arising from the use of any information it contains.

Two-dimensional acoustic particle focusing enables sheathless chip Coulter counter with planar electrode configuration

Carl Grenvall*^a, Christian Antfolk^a, Christer Zoffmann Bisgaard^b and Thomas Laurell*^{ac}

^a Department of Biomedical Engineering, Lund University, Sweden.

E-mail: carl.grenvall@bme.lth.se

^b Foss Analytical A/S, FOSS, Hillerød, Denmark.

^c Department of Biomedical Engineering, Dongguk University, Seoul, Republic of Korea

Abstract

The field of cytometry has grown in scope and importance ever since the early 20th century with leaps in technology introducing the Coulter counter and the flow cytometer. Cytometry methods have brought about a revolution for the medical and biotechnology industry by providing fast and accurate analysis of cell and particle suspensions. Recent developments in the field aim at improving current cytometers and to provide miniaturized low-cost cytometry systems for point-of-care clinical diagnostics or research. In an attempt to address the need for particle positioning which is important for both impedance and optically based cytometers we present a microfluidic system which precisely positions cells and particles, using acoustic forces and subsequently performs measurements using an integrated and simple planar electrode Coulter-type impedance cytometer without the need for sheath flows. Data is presented to show how the acoustic method improves the accuracy of the impedance cytometer when prefocusing is employed to particles and cells (diluted whole blood). Confocal imaging and simulations support the findings and provide the basis for further improvements. The acoustophoretic prefocusing technique opens a path towards small, low cost cytometers while also providing an easy way to improve current systems.

Introduction

In this paper acoustic forces are utilized to address the need for precise positioning of cells and particles in continuous flow to enable low cost chip integrated Coulter counters. When using Coulter type instruments the particle position in relation to the electrical field gradient in the measurement cell is important, and correspondingly, when using light or fluorescent techniques the particle need to be positioned in the focal plane of the light sources and detectors. High throughput cytometry first became available with the introduction of the Coulter principle ^{1,2}. Coulter cytometers count and size particles by measuring the variations in impedance or resistance that the particles cause when displacing a conductive fluid in an electric field. Typically, the electric field is generated across a narrow aperture to maximize the proportional fluid volume displacement. Early research improved the aperture, the flow control and the instruments that quantify the electric pulses caused by the particles ³⁻⁵. The instruments have since been improved by computerization, but not vastly changed until recently, when microfabrication technologies introduced new possibilities in terms of aperture design and electrode configuration in planar microchip formats ⁶.

Notes about how to position particles by the use of nozzles, flow chambers or sheath flow strategies were already included in early cytometer papers and patents. In particular, the ability to position particles using sheath flows is of importance in most cytometers regardless of the detection method, including impedance measurements as well as traditional microscopy or fluorescence flow cytometry, since this not only allows positioning but also prevents clogging, a frequent problem when using small apertures and nozzles⁷⁻⁹. The introduction of chip integrated microfluidic systems made it possible to design new kinds of coulter type instruments, where electrodes could be placed in parallel along or across a microfluidic channel. This type of non-axial electrode configuration was actually included in Coulter's original patent but deemed difficult to implement due to thermal noise¹⁰. The transition to microfluidic systems also facilitated the development of continuous flow based microchip impedance spectroscopy (MIS), a method that allows cell counting and sizing combined with the ability to differentiate between cell types, by measuring impedance across cell membranes and cytosols in high frequency electric fields^{11,12}. Current improvements in the impedance cytometry field can be attributed to improved control of fabrication steps on the micro scale. These include clever electrode configurations, aperture designs and particle positioning methods. Several novel electrode designs have recently been proposed. These include transverse, planar and liquid electrode systems¹³⁻¹⁵. Compared to transverse designs, which depend on precisely fitting top and bottom channel substrates to align the electrodes precisely to each other, the planar configurations are cheaper and easier to fabricate but suffer from sensitivity in the particle positioning during the measurement since the electrical field is non-homogenous¹⁶⁻¹⁸. Hydrodynamic lamination of a non-conductive sheath flow around a conductive sample medium in one- or two-phase systems, to create a fluidic aperture rather than a microfabricated aperture, has also been presented. The technique, while promising in the sense that it is able to produce very narrow adjustable apertures, is sensitive to ion diffusion which causes erroneous measurements, and unstable flow, which requires a more complex fluidic solution¹⁹⁻²¹.

Microfluidic chip cytometry has created new possibilities for the cytometry research field, but also added new challenges since the materials and fabrication process of these chips do not easily yield the kind of macro scale hydrodynamic positioning methods, axisymmetric nozzles and fluid handling techniques, used in larger systems to improve throughput and avoid clogging²²⁻²⁶. Thus new ways of positioning the particles to comply with the planar configurations of chip based microfluidics were presented. These include systems utilizing externally induced electrokinetic, magnetic or optical forces as well as hydrodynamic forces and other ways to manipulate particles by accurate design of the flow channels themselves²⁷⁻³⁶. While able to position particles satisfactorily, these new techniques also have their weaknesses. In order to achieve precise positioning using multiple channel hydrodynamic focusing, the microfluidics systems often get more complex and expensive to produce, requiring an increased number of fabrication steps and several fluid pumps which makes them bulkier and harder to integrate into analytic instruments. High flow rate as in the case of sheet flow configurations may cause stress on cells and thus impact viability. While electric focusing techniques can be used in uncomplicated fluidic systems, they also make the systems more complex due to electrode interference between focusing and sensing electrodes which needs to be addressed with more or less intricate designs^{37,38}.

Acoustophoresis, a method in which particle positions are manipulated using standing wave acoustic forces, is gentle to cells with reports of successful sample particle focusing, separation, sorting, fractionation, trapping, media switching and in-field cell culturing³⁹⁻⁴³. Acoustic forces on

microparticles were first investigated in the late 19th century with improved understanding reported in the mid-20th century⁴⁴⁻⁴⁷. Recent reports on how acoustic forces act on microparticles in a microfluidic channel provide the basis on which the system reported herein was designed⁴⁸. Typical acoustophoretic systems are designed to actuate the primary eigenmodes of the microfluidic channel such that an acoustic half wavelength standing wave is established and the corresponding pressure node is formed in the horizontal or vertical center plane of the channel either because of wall-wall (horizontal focusing) or top-bottom (vertical focusing) resonance. Designs with multiple nodes have also been presented, often in systems with complex biosuspensions in order to control the different types of cells and particles, or to add parallel functionality and increase throughput^{49,50}. Recently several designs that actuate the channel in both planes simultaneously (2D-focusing) have been presented. This can be done either by using two acoustic actuation frequencies, one for each direction, or by designing the channel in such a way that a single frequency can be used to form standing waves in both directions⁵¹⁻⁵⁴. Fundamental developments of sheathless 2D-focusing of particles in flow was described by Goddard et al.⁵⁵ who shortly after realized this in an excellent and unsurpassed work on fluorescence flow cytometry.⁵⁶ This development fuelled the commercial development of the Attune acoustic focusing flow cytometer (Life Technologies). The possibility of precise non-contact spatial localization of particles in flow using bulk acoustic standing waves suggests that acoustic 2D-focusing of particles also could be realized in sheathless chip integrated impedance cytometry.

In this paper we address some of the challenges of chip complexity in MIS systems, required to accomplish sufficient measurement accuracy, by combining a low cost planar electrode design with precise acoustophoretic particle positioning. Rather than striving to create a homogenous electrical field across the impedance measurement zone, we propose the use of a planar electrode configuration with a gradient electrical field and instead ensure that the particles/cells are acoustically aligned to the same location in the electrical field gradient, such that equally accurate impedance measurements can be accomplished as compared to measurements based on standard Coulter instrumentation.

A chip with a single glass channel was designed and fabricated to allow upstream acoustic 2-dimensional prefocusing of cells and particles, aligning these in a uniform position in the channel cross section prior to entering a downstream measurement aperture with two pairs of planar electrodes that allowed single particle differential impedance measurements to be carried out. We present theoretical and experimental data on polystyrene particles and cells (diluted whole blood) that support our claim that the system is able to count and size cells and particles using a standard glass microfabricated Coulter counter orifice with a planar electrode configuration. The acoustic Coulter counter chip is benchmarked against golden standard Coulter counter measurements showing equal or better performance. The work presented here is a continuation of our project in which we aim to develop a chip based low cost acoustophoretic cytometer for milk quality control⁵⁷.

Materials and Methods

Chip design and system setup

The microfluidic chip was designed to support a two dimensional (2D) acoustic focusing pressure node in the center of a straight channel (width: 420 μm height: 150 μm) and was fabricated in glass

by Micronit Microfluidics, the Netherlands. 2D prefocusing was accomplished by simultaneously exciting both the fundamental vertical as well as the horizontal resonance mode of the channel cross section using two piezoceramic transducers (PZ26, Ferroperm) actuated at 2 and 5.3 MHz respectively by a dual channel function generator (AFG 3022B, Tektronix). The system was configured with two transducers, enabling actuation of each resonance mode separately when investigating system performance with no ultrasound, only vertical (1DV), only horizontal (1DH) and 2D-prefocusing (Fig. 2a). The 5.3 MHz signal was amplified to a peak-to-peak amplitude of 12 V using an in-house designed RF amplifier while the corresponding 2 MHz signal was operated at 7 V_{pp} using only the signal generator. The transducers were glued to an aluminium block (10 x 10 x 20 mm), acting as a heat sink and, and was docked to the glass chip. Glycerol was applied as an acoustic coupling layer between the aluminium block and the glass chip.

The chip was placed in a holder (Fluidic Connect 4515, Micronit Microfluidics), providing fluidic and electronic access to the chip, using threaded PEEK connectors. The fluidic network, Teflon tubing with 0.3 mm inner diameter (TFE 58697-U, Supelco), connected the 1 ml sample syringe (BD Plastipak, Becton Dickinson) to the channel inlet and the channel outlet to an open waste container. Constant sample flow was generated using a syringe pump (Nemesys, Cetoni).

The mid-section of the microfluidic channel was narrowed to an aperture (width: 80 μm height: 35 μm) where planar electrodes was patterned across the flat bottom for the impedance measurements. A forked signal electrode was placed between three pairs of sensing electrodes, allowing for optional spatial electrode distances. In this paper the electrode pair closest to the signal electrode was used. Each electrode was 200 nm thick and 20 μm wide and placed with a center-center distance of 50 μm (30 μm of non-patterned glass between each electrode). The signal electrode fork was 80 μm wide center-center. The fluidic network was connected to ground and all cables were shielded in order to minimize external noise (predominantly 50 Hz). Signal generation and MIS signal detection was carried out using an impedance spectroscope (HF2IS, Zürich Instruments) operated in differential mode. Current signals from the sensing electrodes were amplified and converted to voltage using a transimpedance current amplifier (HF2TA, Zürich Instruments) prior to data acquisition. Pulse data was recorded on a PC using pulse edge triggered software (LabOne, Zürich Instruments) in order to minimize raw data stream sizes and allow long term measurements (230 kSa/s, 40 μs TC). The data was exported to MATLAB (MATLAB, Mathworks) for further analysis. An overview of the experimental setup can be seen in figure 1.

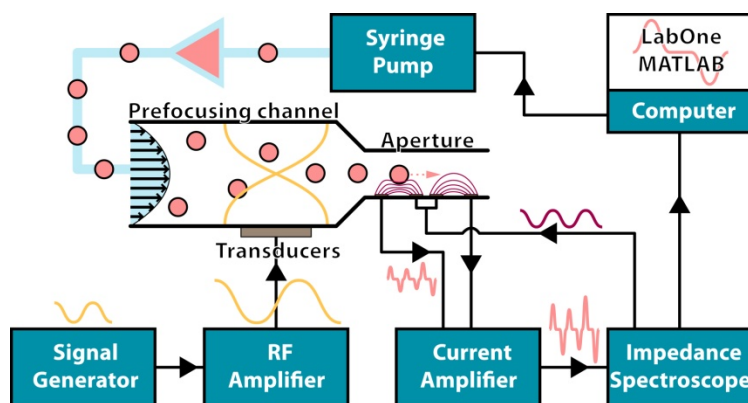


Figure 1. Schematic of the experimental setup. A computer controlled syringe pump maintained a stable flow in the channel. The sample suspension was pumped into the chip where the particles/cells were acoustophoretically prefocused in a single flow velocity vector using a 2-dimensional acoustic standing wave field prior to entering the MIS aperture. MIS signal generation and readout was performed by an impedance spectroscopy, followed by MathLab analysis.

The primary acoustic radiation force focuses particles into either acoustic pressure nodes or antinodes according to their acoustic contrast factor. The contrast factor depends on differences in the density and compressibility of the particles and the surrounding medium⁵⁸. Dense particles (i.e. cells) have positive contrast, and consequently focus into the nodes, when suspended in most commonly used flow media like water.

When isotropically etched glass is used as channel material the resulting channel walls will be rounded. This results in an acoustic field that is more complex as compared to straight wall geometries cf.⁵³. Although, the acoustic focusing performance of isotropically etched glass channel geometries operated in 1 dimension horizontal resonance mode have previously been investigated, a COMSOL (Multiphysics 4.3a, COMSOL) simulation of both the fundamental vertical and horizontal resonance mode was performed in this study (Fig. 3), and compared to the corresponding experimentally derived confocal data (Fig. 5)⁵⁹.

Impedance based flow cytometry

A planar electrode configuration allows all electrodes to be placed on a single substrate bonded directly to a substrate in which the flow channel is fabricated. This makes the manufacturing process less complicated (cheaper) but in turn strictly requires that all particles are passing through the same spatial position in the aperture cross section, commonly accomplished by a more complex fluidic set-up using a 2-dimensional sheet flow. In terms of accuracy, planar configurations are equal to transverse systems, but only when the particle positioning can be controlled, since the planar systems are more prone to erroneous readings due to varying particle positions (Fig. 2b). By applying an AC-field across this suspension, the passing particles will induce resistance changes in the suspension as they flow past the electrode pairs, giving rise to pulses from which particle sizes can be derived (Fig. 2c)¹⁰. The MIS was operated at an amplitude of ~ 2 V a frequency of ~ 1 MHz, at which it can be described as a Coulter counter, where the changes in suspension resistance is

dominated by conductive fluid volume changes (particle size) rather than membrane capacitance or cytosol resistance contributions (Fig. 2d). The data generated by the MIS was analyzed using Matlab (Matlab 2012b, Mathworks). The in-phase signal from the impedance analyzer was used in combination with a high-pass filter ($f_c = 5\text{Hz}$), eliminating the DC component. The peaks and valleys of the signal (corresponding to a particle traversing the electrodes) were identified and used in the subsequent signal analysis. Amplitude, time of passage between electrodes (TOP), and velocity for all events were calculated. For further understanding the MIS was also simulated. The flow-velocity profile for the channel geometry was calculated in COMSOL using the geometries in the experimental channel. The impedance signal was simulated using COMSOL, by modelling a particle passing through the channel at different positions (Fig. 3). All boundaries except the electrodes were set to be insulators and the ends of the flow-channel were set to be periodic continuity boundaries. A 1 V signal was applied to the middle electrode and the outer electrodes were set to 0 V. The current density on each of the ground electrodes was integrated across the electrode area to give the total current and the current values were subtracted to give the differential current signal. This value was used as the impedance signal.

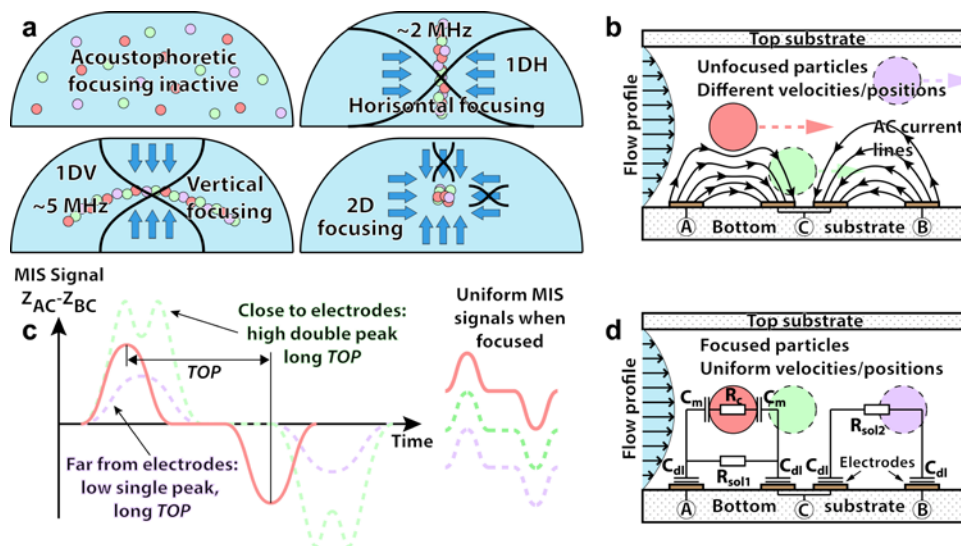


Figure 2. Schematics of 2D acoustophoretic prealignment in MIS. Vertical and horizontal focusing is combined to create a 2D focusing node in an acoustophoretic system based on isotropically etched glass channels (a). MIS readout in planar electrode configurations is sensitive to particle positioning due to the heterogeneity of the electric field (b-c). By analyzing the pulse curve shape it is possible to determine approximately where in the channel a particle was travelling (c). At $\sim 1\text{MHz}$ measurement frequency, impedance signal variations are mainly caused by the displaced conductive fluid (R_{sol}) rather than the cell membrane conductivity (C_m) or cytosol resistance (R_c), thus making the system suited for particle size measurements (d).

Model particle suspensions and biofluids used in the experiments

Model particle samples consisted of polystyrene beads (Fluka, Sigma-Aldrich) suspended in saline (0.9% NaCl in Milli-Q water). A suspension containing 7 μm polystyrene (PS) beads was used for initial proof-of-principle experiments which included a set of runs in which different bead concentrations were analyzed in order to find optimal concentration conditions with respect to maximized throughput and minimized number of doublets. 7 μm PS beads were also used to evaluate system performance during runs with no ultrasound (0D), sidewall-sidewall standing wave ultrasound (1DH), top-bottom standing wave ultrasound (1DV) and simultaneous 1DH and 1DV ultrasound, resulting in two dimensional focusing (2D). A suspension with 3, 5 and 7 μm PS beads was used to evaluate the size measurement performance of the chip Coulter counter. Measurement performance on biofluid samples was evaluated by diluting whole blood 1:10000 using normal saline spiked with 7 μm beads. Flow rate was set to 10 $\mu\text{l}/\text{min}$ for the 7 μm bead samples and 5-7 $\mu\text{l}/\text{min}$ for the bead mix and blood experiments, assuring laminar flows conditions. For comparison of the chip MIS operated in Coulter counter mode the suspensions were analyzed in a golden standard Coulter counter (Multisizer 3, Beckman Coulter).

Confocal imaging

For better understanding and confirmation of the acoustic focusing modes used to actuate the chip, z-mode confocal image reconstructions of the particle focusing were generated (Fig. 5a-d). Green fluorescent 4.8 μm PS beads (Fluoro-Max G0500, Thermo Scientific) were run through the channel during 0D, 1DH, 1DV and 2D acoustophoretic actuation. For visualization of beads and channel boundaries fluorescent images were captured using a confocal microscope system (Fluoview 300 running on a BX51WI microscope, Olympus) with dual lasers (PS-Argon-Ion and PS-HeNe, Melles Griot).

Results and Discussion

Simulation results of acoustic and impedance chip properties

The acoustic simulations showed that a 150x420 μm rounded wall geometry would allow 0D, 1DH, 1DV and 2D experiments to be carried out when actuating the chip at frequencies close to those previously examined (2 and 5 MHz) (Fig. 3a and b). The modeling predicted a vertical $\lambda/2$ -resonance top to bottom of the channel at 5.3 MHz while the sidewall-sidewall, horizontally particle focusing standing wave, was predicted at 2.0 MHz. By simultaneous actuation of the channel using these two frequencies, a 2D focusing node in the center of the channel should form.

The impedance simulations were integral for understanding and analyzing experimental data. The results show that a particle travelling close to the electrodes (positions 1-3, Fig 3d) induces a comparatively high amplitude signal with a double peak, while particles far away from the electrodes (positions 10-13) induce low single peak signals, analogous to the signal profiles reported by Morgan et al.⁶⁰. Estimating the particle size based on the peak height would in these cases result in particles to be interpreted as either too large or too small as compared to particles of the same size passing in other parts of the channel. Particles travelling in the slow flow rate domains (positions 1-3, 4, 7, 12,

13) display longer TOP compared to fast travelling particles in the center of the channel (6, 8-9, 11). By employing 2-dimensional acoustophoretic prefocusing, locating the particles in the center of the channel (position 9), the errors caused by spatial dependence of the particles during the impedance measurement are eliminated.

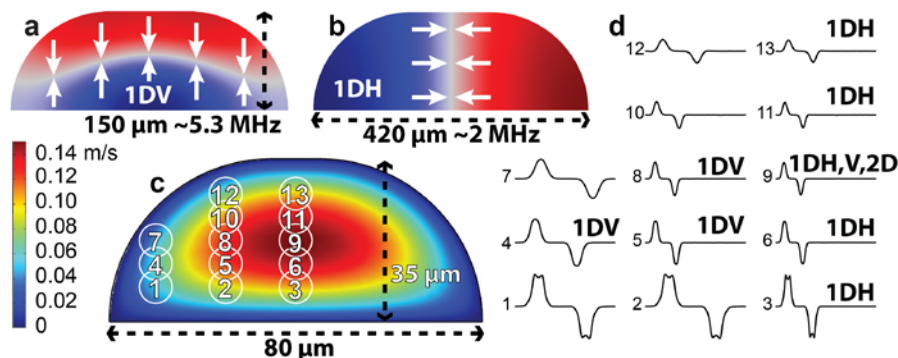


Figure 3. Simulation results. COMSOL simulations of acoustic eigenmodes predicted the vertical and horizontal resonance modes at ~ 5.3 MHz and ~ 2.0 MHz respectively (a and b). Simulations of the impedance pulse shape show the effects of varying spatial particle positions in the channel cross section (c and d) Channel dimensions were $150 \times 420 \mu\text{m}$ for the acoustic simulation and $80 \times 35 \mu\text{m}$ for the impedance simulation.

Initial suspension concentration experiments

The microchannel consisted of a 19 mm long pre-focusing section in which particles could be simultaneously focused both laterally and vertically. When defining the design specification the cross section dimensions of the prefocusing channel were chosen according to the acoustic eigenmode simulations. The prefocusing channel was followed by a narrow aperture section ($80 \times 35 \mu\text{m}$ and 1.5 mm long) with electrodes patterned across the flat channel bottom to enable Coulter counter measurements (Fig 4). The 2D-acoustic prefocusing confined the particles to a well-defined flow velocity vector in the channel center, as verified by experimental data showing a narrow velocity distribution and uniform impedance peak shapes, i.e. particles pass the electrode region in the same location of the channel cross-section^{11,60}.

The initial MIS experiments were carried out to determine the optimal particle concentrations for subsequent experiments. A low particle concentration results in high percentage of usable events (minimizing the risk for doublets – having multiple particles in the measurement zone simultaneously), but makes the analysis slow when counting large number of events. Conversely, a high particle concentration allows for rapid analysis but leads to an increase in number of unusable events. The concentration study showed that ~ 300 particles/ μl is sufficient to achieve $\geq 90\%$ usable events (Fig. 4c). Calculations of the probability of having multiple Poisson-distributed particles in a fluid volume equivalent to the measuring zone was carried out given varying concentrations and supported the experimental finds (Fig. 4c). At a concentration of 38 particles/ μl the proportion of usable events was close to 99%. The subsequent experiments in this paper were performed at

concentrations of 100-300 particles/ μl since it allowed for a combination of relatively high usable event ratios and rapid analysis.

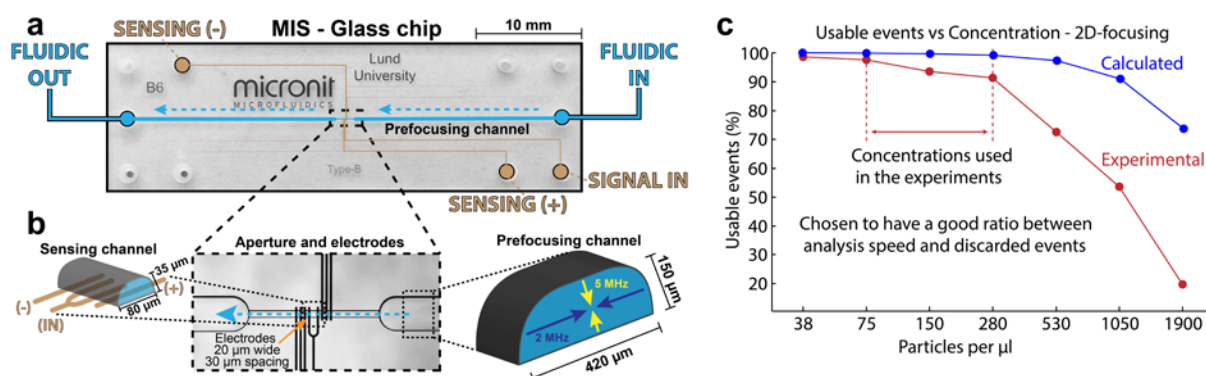


Fig 4. Channel design and initial results. The 45x15 mm glass chip included a prefocusing channel (19 mm long) and a sensing channel (1.5 mm long) (a). The prefocusing channel (420 x 150 μm) was designed to focus particles in 2-dimensions (b-right). The sensing channel was 80x35 μm across which electrodes were patterned to perform measurements on cell-sized particles (1-20 μm in diameter) (b-left). Initial experiments and were carried out to determine optimal suspension concentrations and optimal concentrations were determined to be 100-300 particles/ μl , also supported by calculating the probability of having two or more Poisson-distributed particles in the sensing channel simultaneously given varying suspension concentrations (c).

Impact of acoustophoretic prefocusing on MIS performance - No ultrasound

When a sample of 7 μm polystyrene particles was perfused through the channel without acoustophoretic prefocusing, particles were evenly distributed over the channel cross section. This distribution was also confirmed by confocal imaging (Fig. 5a) and resulted in large variations in pulse amplitudes and TOP data. A pulse amplitude vs. velocity (TOP-data) plot (AV-plot) illustrates the relationship between particle positions and the impedance signal they induced (Fig. 5i). The resulting AV-plot share the boomerang shape with the simulated data of 50 000 events (Fig. 5e), which was consistent throughout the experiments, with the fastest travelling beads at its vertex and with beads positioned either below or above the channel center visible along the boomerang sides. In accordance with simulations, beads that travel close to the electrodes have low velocities with high pulse amplitudes, thus positioned far from the vertex along the right side of the data distribution in the AV-plot while the equally slow travelling particles far from the electrodes at the channel top have lower pulse amplitudes and are visible in the left side of the data distribution of the AV-plot (Fig. 3d positions 3 and 13).

1-dimensional horizontal focusing (sidewall-sidewall) - 1DH

When actuating the channel using the horizontal resonance, sidewall-sidewall, the confocal imaging confirmed that the beads were focused in a thin ribbon from top to bottom at the center of the

channel (Fig. 5b), in agreement with the COMSOL simulations. In this case the peak amplitude (V) depends on the position in the vertical direction of the channel and the particle velocity measurement (TOP) in the laminar flow profile is reflected in the skewed parabolic shape of the measured data distribution (Fig 5f). The deviation from a true parabolic shape is due to the fact that the vertical electrical field gradient is not linear. The same distribution is also seen in the corresponding COMSOL modelling (Fig 5j).

1-dimensional vertical focusing (top-bottom) - 1DV

Acoustic actuation of the channel with a top-bottom vertical standing wave focused particles into a curved horizontal sheet across the channel, as predicted from simulations and confirmed by confocal imaging (Fig. 5c). This is the first experimental verification of a curved shape of the ultrasonic $\lambda/2$ standing wave pressure nodal line in microfluidic channels with rounded side-walls. The curve phenomenon is an effect of the channel geometry which alters the resonance criteria close to the rounded walls. The combination of the curved particle sheet and the rounded wall geometry makes the AV-data points widely distributed under the parabolic shaped data boundary since it is not possible to directly translate a certain velocity to a point on either side of the vertical symmetry axis of the channel (contrary to the top-bottom regime of the straight 1DH particle ribbon) (Fig. 5g and k). The different shapes of the parabolic data boundaries between the simulated and experimental data is interpreted as being caused by slight deviations in the modelled electrical field gradient and the actual gradient in the microchannel.

2D ultrasound

When operating the system in the 2-dimensional acoustophoretic focusing mode the confocal imaging showed particles localized to the superimposed nodal point of the horizontal and vertical resonances (Fig. 5d). The impedance measurement data in the corresponding AV-plot were all confined to a point at the vertex of the parabolic distribution profile, Fig 5l. All of the $\sim 30\,000$ particles that were analyzed were clustered in the 2-D nodalpoint, agreeing well with the corresponding modelling data (Fig 5h). For comparison with commercial instruments and previously presented systems using optical or impedance based cytometry a threshold was added (Fig. 5l) to remove doublets. The procedure removed 3.8% of the events, corresponding well with expected levels of unusable events ($<10\%$) for the particle concentration interval used. The coefficient of variation (CV) for the remaining events (96.8%) was 2.04% (cube root of CV for pulse amplitudes). This value is on par or better than size CV's reported on similar size beads (6-7 μm) by other groups that use impedance or optically based cytometry in combination with either acoustic, inertial or electric forces to position particles. Reported CV's include 1.6% (inertial focusing of 6 μm particles combined with transverse electrode MIS)⁶⁰ and 1.8% (dielectric focusing of 6 μm particles combined transverse electrode MIS)¹⁸ for impedance size measurements and 2.56% (bulk acoustic wave focusing of 10 μm particles combined with fluorescent flow cytometer)⁵⁶ and 10.9% (surface acoustic wave focusing of 10 μm particles combined with fluorescent flow cytometer)⁶¹ for fluorescence amplitude CV's. Groups often report CV's on events in a distinct amplitude distribution and the size CV of 2D focused particle events using this criterion was 1.50% with 95.0% events remaining (Fig. 5l), which is less than the stated CV ($<2.0\%$) from the manufacturer (Sigma), measured using a Multisizer, the same golden standard commercial instrument that we benchmark our system against in the experiments described below. It should be noted that fluorescence cytometer measurements

depend on particle size as well as fluorescent intensity which makes it difficult to compare particle focusing precision between the two using only amplitude CV's.^{18,35,56}

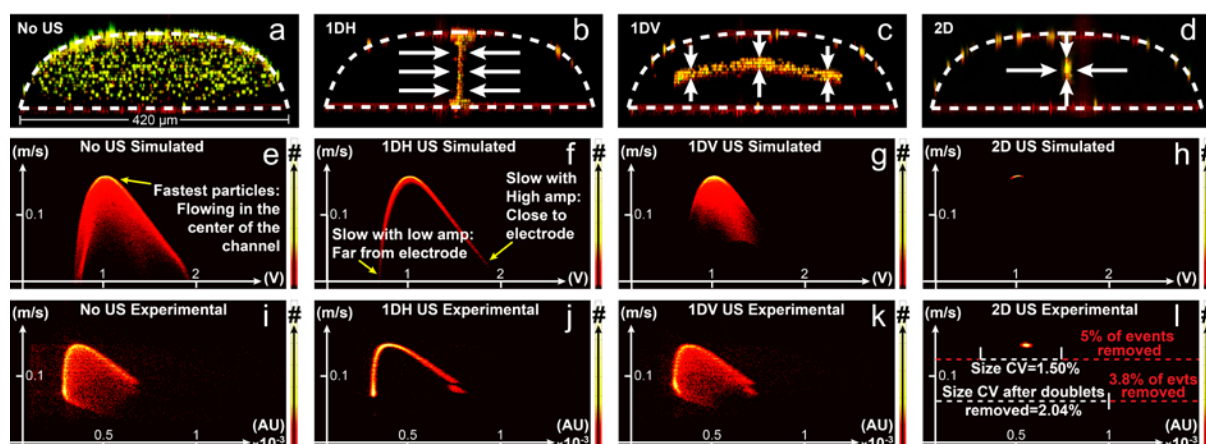


Fig 5. Simulated (50×10^3 events) and experimental (30×10^3 events) MIS data for $7 \mu\text{m}$ beads during OD (No US), 1DH, 1DV and 2D modes of operation as well as z-mode confocal imaging. In OD mode beads are distributed across the channel cross section, with large variations in velocities and distance to the electrodes (a, e, i). In 1DH mode beads are aligned in a vertical ribbon (b) from top to bottom, yielding a parabolic-like shape (linked to the laminar flow profile) of the data distribution in the AV-plot (f, j). In 1DV mode beads are aligned in a curved sheet, where the curvature of the sheet results in a broad distribution of data points underneath the parabolic shaped delineation (c, g, k). In 2D focusing mode the beads are all focused in the center of the channel, travelling at the same velocity and distance from the electrodes, resulting in minimized variations in the data point distribution in the AV-plot, ideally only varying in amplitude due to size differences of the beads (d, h, l). For comparison to size sensitivity CV's in other systems two sets of thresholds were added, one removed pulses above 1.0×10^{-3} AU (doublets) and the other removed pulses outside the $0.25\text{--}0.75 \times 10^{-3}$ AU range (removing events outside the distinct event distribution at $\sim 0.5 \times 10^{-3}$ AU). The remaining 96.2 and 95.0% events had particle size CV's of 2.04 and 1.50% respectively.

Size discrimination

A mixture of 3, 5 and $7 \mu\text{m}$ PS beads passing through the channel was investigated. Derived data from experiments with no ultrasound indicated three partly overlapping populations and the corresponding amplitude and TOP measurements within each population also varied significantly (Fig. 6a, b, c). In contrast, with 2D acoustic focusing three distinct focal regions emerged in the AV-plot, (Fig. 6e) and the size histogram displayed fully separated size distributions (Fig. 6f). Particles were all travelling at similar velocities (Fig. 6d) and the different particle size induced pulse amplitudes corresponding to the three particle volumes. The samples were also analyzed using a Multisizer 3, showing comparable data to the MIS recorded data (Fig 6h vs b and f).

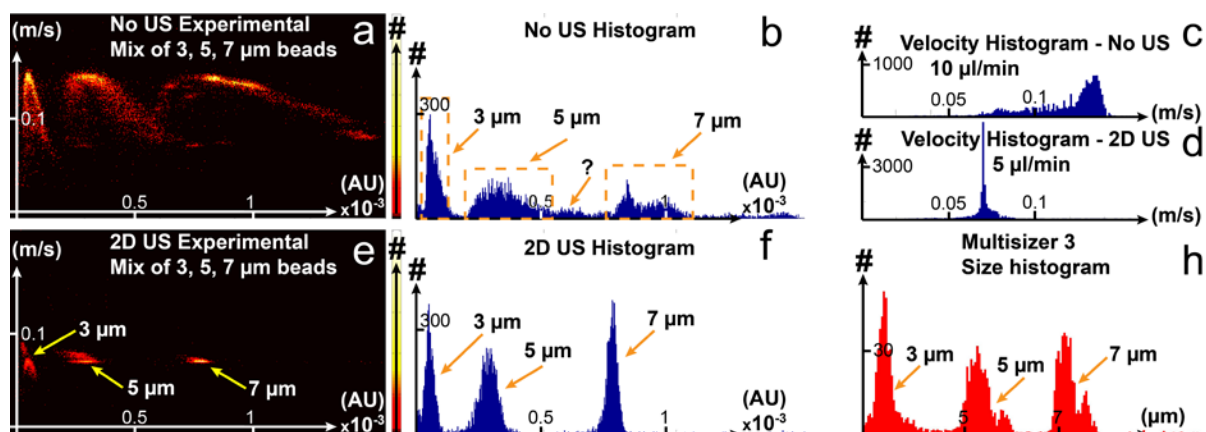


Fig 6. AV-plots and histograms from 2D-prefocused and unfocused samples with a mixture of 3, 5, 7 μm PS beads (17×10^3 events). An AV-plot of the unfocused beads show data with wide distributions for each bead size (a) while the acoustically prefocused sample shows each population clearly focused in three distinct zones (e), also visible in the velocity histograms (c vs d). The corresponding size histograms also demonstrates the importance of the 2D-prefocusing c.f. (b) and (f) and the Golden standard reference data obtained from the Multisizer 3 Coulter counter (h).

Blood spiked with 7 μm PS beads

A blood/bead suspension was run through the chip with 2D prefocusing either active or inactive until 20 000 events were recorded for each setting. Without prefocusing it was barely possible to differentiate between the bead and blood cell population (mainly erythrocytes), (Fig. 7a and b). However, when the prefocusing was activated the data showed a distinct difference between the two populations (Fig. 7e and f). The blood population showed slightly less conformity in amplitude data (size) while the velocities were consistently uniform for both populations. This is also reflected in the broader cell volume distribution in the RBC population as measured by the reference Coulter counter, Fig 7h. Velocity histograms from the experiments with and without prefocusing show the significant improvement in velocity variations between prefocused and unfocused samples (Fig. 7c vs d). The samples were also analyzed in a Multisizer 3 and the histograms were compared to histograms generated from the MIS experiments with prefocusing activated (Fig. 7f vs 7h), showing good agreement with the golden standard instrument both in terms of particle size distribution and total number of particles in each population.

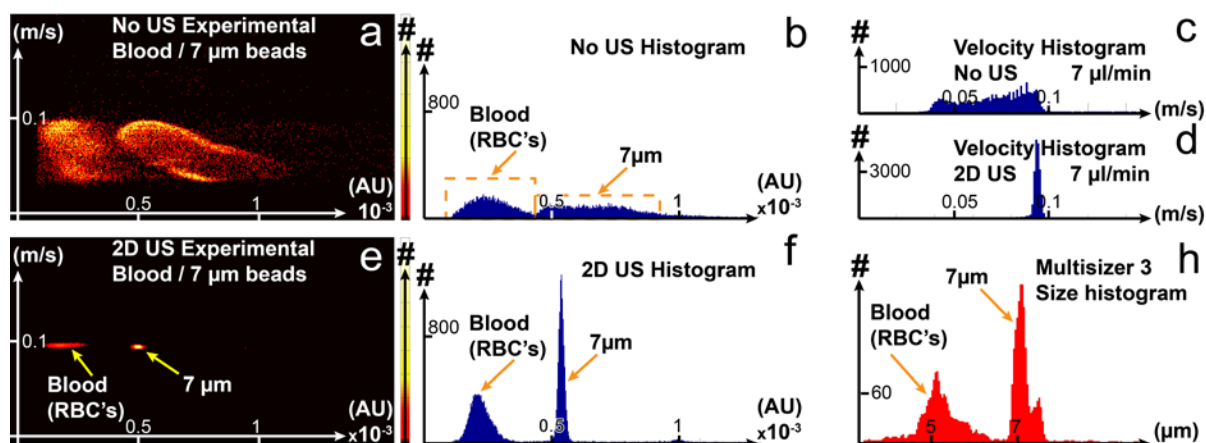


Fig 7. Experimental data for a mixture of diluted whole blood and 7 μm beads. In the unfocused sample it is barely possible to distinguish two populations of particles with different sizes (volume difference between RBC's and 7 μm PS beads) and the histogram suggests that sizes overlap slightly (a and b). The difference in size between the RBC's and the PS beads become apparent with prefocusing activated (e and f). As seen with the pure bead samples the blood/bead mix also show significantly less variation in speed when they are focused (c, d). The prefocused blood/bead data (f) compares well with the benchtop Coulter counter (h).

Conclusion

We have developed a microchip impedance spectrometer (MIS) with planar electrodes in a single sided configuration, which uses acoustophoretic prefocusing of cells and particles to circumvent the need for sheet flow alignment. Experimental results illustrate the importance of particle positioning in these systems, specifically in MIS systems that uses a planar electrode configuration. The MIS was able to analyze single and mixed size bead suspensions as well diluted whole blood and data correlates well with golden standard Coulter counter measurements. The combination of acoustophoretic focusing and planar electrodes enables a simple route to fabricate chip integrated Coulter counters and impedance spectrometry systems by processing the microchannels in one glass layer and the measurement electrodes in a single lithography step on the covering glass slide. The design alleviates the need for elaborate channel designs with sheet flow functionality, intricate electrode configurations and more advanced flow control.

Acknowledgements

The authors would like to thank the following organizations and companies for their financial support: FOSS A/S, FORMAS Tvärlivs, VINNOVA IFFH CellCARE, Swedish Research Council (637-2013-444), Stiftelsen Olle Engkvist Byggmästare.

References

1. W. H. Coulter, 1953.
2. A. Moldavan, *Science* (80-.), 1934, **80**, 188–189.

3. H. E. Kubitschek, *Nature*, 1958, **182**, 234–235.
4. C. F. T. Mattern, *J. Appl. Physiol.*, 1957, **10**, 56–70.
5. R. H. Berg, 1966.
6. W. R. Hogg, *US Pat. 3936739*, 1976.
7. P. J. Crosland-Taylor, *Nature*, 1953, **171**, 37–38.
8. P. N. Dean, D. Pinkel, and M. L. Mendelsohn, *Biophys. J.*, 1978, **23**, 7–13.
9. W. A. Bonner, H. R. Hulett, R. G. Sweet, and L. A. Herzenberg, *Rev. Sci. Instrum.*, 1972, **43**, 404–409.
10. M. Koch, A. G. R. Evans, and A. Brunnschweiler, *J. Micromechanics Microengineering*, 1999, **9**, 159–161.
11. S. Gawad, L. Schild, and P. H. Renaud, *Lab Chip*, 2001, **1**, 76–82.
12. D. Holmes and H. Morgan, *Anal. Chem.*, 2010, **82**, 1455–61.
13. T. Sun and H. Morgan, *Microfluid. Nanofluidics*, 2010, **8**, 423–443.
14. L. I. Segerink, A. J. Sprenkels, J. G. Bomer, I. Vermes, and A. van den Berg, *Lab Chip*, 2011, **11**, 1995–2001.
15. C. Bernabini, D. Holmes, and H. Morgan, *Lab Chip*, 2011, **11**, 407–12.
16. K. C. Cheung, M. Di Berardino, G. Schade-Kampmann, M. Hebeisen, A. Pierzchalski, J. Bocsi, A. Mittag, and A. Tárnok, *Cytometry. A*, 2010, **77**, 648–66.
17. D. Barat, D. Spencer, G. Benazzi, M. C. Mowlem, and H. Morgan, *Lab Chip*, 2012, **12**, 118–26.
18. G. Mernier, E. Duqi, and P. Renaud, *Lab Chip*, 2012, **12**, 4344–9.
19. M. Nasir, D. T. Price, L. C. Shriver-Lake, and F. Ligler, *Lab Chip*, 2010, **10**, 2787–95.
20. C. Bernabini, D. Holmes, and H. Morgan, *Lab Chip*, 2011, **11**, 407–12.
21. M. Evander, A. J. Ricco, J. Morser, G. T. a Kovacs, L. L. K. Leung, and L. Giovangrandi, *Lab Chip*, 2013, **13**, 722–9.
22. T. M. Squires and S. R. Quake, *Rev. Mod. Phys.*, 2005, **77**.
23. G. M. Whitesides, *Nature*, 2006, **442**, 368–73.
24. E. Verpoorte, *Lab Chip*, 2003, **3**, 42N–52N.
25. L. Y. Yeo, H.-C. Chang, P. P. Y. Chan, and J. R. Friend, *Small*, 2011, **7**, 12–48.

26. D. a Ateya, J. S. Erickson, P. B. Howell, L. R. Hilliard, J. P. Golden, and F. S. Ligler, *Anal. Bioanal. Chem.*, 2008, **391**, 1485–98.
27. a Wolff, I. R. Perch-Nielsen, U. D. Larsen, P. Friis, G. Goranovic, C. R. Poulsen, J. P. Kutter, and P. Telleman, *Lab Chip*, 2003, **3**, 22–7.
28. N. Demierre, T. Braschler, P. Linderholm, U. Seger, H. van Lintel, and P. Renaud, *Lab Chip*, 2007, **7**, 355–65.
29. C. Simonnet and A. Groisman, *Appl. Phys. Lett.*, 2005, **87**, 114104.
30. N. Sundararajan, M. S. Pio, L. P. Lee, and A. A. Berlin, *J. Microelectromechanical Syst.*, 2004, **13**, 559–567.
31. D. P. Schrum, C. T. Culbertson, S. C. Jacobson, and J. M. Ramsey, *Anal. Chem.*, 1999, **71**, 4173–7.
32. D. Di Carlo, *Lab Chip*, 2009, **9**, 3038–46.
33. G. Blankenstein and U. Darling Larsen, *Biosens. Bioelectron.*, 1998, **13**, 427–438.
34. A. Ashkin, *Phys. Rev. Lett.*, 1970, 24–27.
35. D. Spencer, G. Elliott, and H. Morgan, *Lab Chip*, 2014, **14**, 3064–3073.
36. M. Shaker, L. Colella, F. Caselli, P. Bisegna, and P. Renaud, *Lab Chip*, 2014, **14**, 2548–55.
37. J. Voldman, *Annu. Rev. Biomed. Eng.*, 2006, **8**, 425–54.
38. R. Pethig, *Biomicrofluidics*, 2010, **4**.
39. J. J. Hawkes and W. T. Coakley, *Sensors Actuators B Chem.*, 2001, **75**, 213–222.
40. A. Nilsson, F. Petersson, H. Jönsson, and T. Laurell, *Lab Chip*, 2004, **4**, 131–5.
41. F. Petersson, A. Nilsson, C. Holm, H. Jonsson, and T. Laurell, *Lab Chip*, 2005, **5**, 20–2.
42. J. Hultström, O. Manneberg, K. Dopf, H. M. Hertz, H. Brismar, and M. Wiklund, *Ultrasound Med. Biol.*, 2007, **33**, 145–51.
43. M. a Burguillos, C. Magnusson, M. Nordin, A. Lenshof, P. Augustsson, M. J. Hansson, E. Elmér, H. Lilja, P. Brundin, T. Laurell, and T. Deierborg, *PLoS One*, 2013, **8**, e64233.
44. A. Kundt, *Philos. Mag.*, 1868, **35**, 41–48.
45. Lord Rayleigh, *Philos. Mag.*, 1902, **3**, 338–346.
46. L. V. King, *Proc. R. Soc. London, Ser. A (Mathematical Phys. Sci.)*, 1934, **147**, 212–240.
47. L. P. Gorkov, *Sov. Phys. Dokl.*, 1962, **6**, 773–775.

48. R. Barnkob, P. Augustsson, T. Laurell, and H. Bruus, *Lab Chip*, 2010, **10**, 563–70.
49. C. Grenvall, P. Augustsson, J. R. Folkenberg, and T. Laurell, *Anal. Chem.*, 2009, **81**, 6195–6200.
50. M. E. Piyasena, P. P. Austin Suthanthiraraj, R. W. Applegate, A. M. Goumas, T. a Woods, G. P. López, and S. W. Graves, *Anal. Chem.*, 2012, **84**, 1831–9.
51. O. Manneberg, S. Melker Hagsäter, J. Svennebring, H. M. Hertz, J. P. Kutter, H. Bruus, and M. Wiklund, *Ultrasonics*, 2009, **49**, 112–9.
52. P. Augustsson, C. Magnusson, M. Nordin, H. Lilja, and T. Laurell, 2012.
53. M. Nordin and T. Laurell, *Lab Chip*, 2012, **12**, 4610–6.
54. O. Jakobsson, C. Grenvall, M. Nordin, M. Evander, and T. Laurell, *Lab Chip*, 2014, **14**, 1943–50.
55. G. Goddard, J. C. Martin, S. W. Graves, and G. Kaduchak, *Cytometry. A*, 2006, **69**, 66–74.
56. G. R. Goddard, C. K. Sanders, J. C. Martin, G. Kaduchak, and S. W. Graves, *Anal. Chem.*, 2007, **79**, 8740–6.
57. C. Grenvall, J. R. Folkenberg, P. Augustsson, and T. Laurell, *Cytom. Part A J. Int. Soc. Anal. Cytol.*, 2012, **81**, 1076–83.
58. H. Bruus, *Lab Chip*, 2012, **12**, 1014–21.
59. M. Evander, A. Lenshof, T. Laurell, and J. Nilsson, *Anal. Chem.*, 2008, **80**, 5178–85.
60. D. Spencer and H. Morgan, *Lab Chip*, 2011, **11**, 1234–9.
61. Y. Chen, A. A. Nawaz, Y. Zhao, P.-H. Huang, J. P. McCoy, S. J. Levine, L. Wang, and T. J. Huang, *Lab Chip*, 2014, **14**, 916–23.